



Adsorption of ciprofloxacin from aqueous solution onto synthesized NiO: isotherm, kinetic and thermodynamic studies

Davoud Balarak^a, Amir Hossein Mahvi^b, Moo Joon Shim^c, Seung-Mok Lee^{c,*}

^aDepartment of Environmental Health, Health Promotion Research Center, School of Public Health, Zahedan University of Medical Sciences, Zahedan, Iran, email: dbalarak2@gmail.com

^bCenter for Solid Waste Research, Institute for Environmental Research, Tehran University of Medical Sciences, Tehran, Iran, email: ahmahvi@yahoo.com

^cDepartment of Environmental Engineering, Catholic Kwandong University, Gangneung 25601, Republic of Korea, Tel. +82-10-8891-7635; emails: leesm@cku.ac.kr (S.M. Lee), moojoonshim@gmail.com (M.J. Shim)

Received 19 March 2020; Accepted 23 September 2020

ABSTRACT

In the present study, the adsorption behavior of ciprofloxacin (CIP) from aqueous solution, using NiO nanoparticles (synthesized by the sol-gel method) was studied at batch experiments. A number of parameters (e.g., temperature, adsorbent dosage, contact time, pH, and initial CIP concentrations) were studied. The best efficiency for the removal of CIP was obtained by 99.2%. The optimal parameters used here were the temperature of 50°C, synthesized NiO dosage of 1 g/L, concentration 10 mg/L at contact time 90 min, and pH = 3. In order to study the kinetics of adsorbent, the pseudo-first-order, pseudo-second-order, and intraparticle diffusion models were applied. According to the pre-determined correlation coefficients (R^2), the pseudo-second-order kinetic model showed a better correlation between the kinetic behaviors of the adsorbent. Thermodynamic experiments showed that the CIP adsorption was endothermic. The negative values of ΔG° indicate the spontaneous nature of the adsorption. The increased randomness was attributed to the adsorption process based on the positive entropy change. The equilibrium data were tested with Langmuir, Freundlich, Redlich–Peterson, Dubinin–Radushkevich, and Temkin isotherm at four different temperatures and it was observed that the Langmuir isotherm was best fitted in the adsorption of CIP.

Keywords: Ciprofloxacin; NiO nanoparticle; Adsorption; Isotherm; Kinetic; Thermodynamic

1. Introduction

Due to the rapid growth of the population, the demand for freshwater is becoming limited and increasing the scarcity day by day [1,2]. The toxicity of chemicals that may cause adverse effects for human health and that has become a critical concern [3,4].

Antibiotics as one of the most important groups of pharmaceutical compounds that are extensively used for the prevention or treatment of diseases [5].

In general, antibiotics are released to water bodies through two main paths: (i) excretion of antibiotics unmetabolized portion from human and animal bodies through feces or urine and (ii) antibiotics direct disposal as waste. Because only partial removal of these compounds can take place in wastewater treatment plants, the treated outlet effluents from these systems still contain amounts of antibiotics [6,7]. For instance, antibiotics in drinking water result in unknown health effects by chronic low-level exposure if antibiotics are not removed during the process of water

* Corresponding author.

purification and exist in the drinking water of consumers [8]. Furthermore, antibiotics can be a reason for bad odors and skin problems and may lead to the microbial resistance against pathogens or the extinction of organisms that are available during the water treatment process [9].

Ciprofloxacin (CIP) (Fig. 1), a common human and veterinary fluoroquinolone antibiotic, has been used for decades to prevent human and animal infections [9,10]. CIP enters into the water column through incomplete metabolism from the human body and/or by wastewater discharged from pharmaceutical companies. Thus, CIP can exist in waters at hundreds of ng/L to $\mu\text{g/L}$ levels. The pK_a values for CIP are 5.90 ± 0.15 and 8.89 ± 0.11 for the carboxylic acid group and the basic-N-moiety, respectively; therefore, it is formed as a cation, zwitterion and anion in soils and waters (Fig. 2) [11,12].

Thus, the wastewater from drug manufacturing plants should be considered as a significant risk, and technology to eliminate the risk of antibiotics should be applied to save humans and environments [13]. Recently, many methods had been tried to remove the antibiotics that appeared in the other environment [14]. These include coagulation and sedimentation, biodegradation, photo-transformation, electrochemical, chlorination, ozonation, and nanofiltration through membranes [15,16]. These methods effectively removed antibiotics but were less popular due to their high cost and complexity [17,18]. Besides these methods, adsorption has been proven to be an effective method due to its

good application to high concentrations of the adsorbed materials and also for its high removal and low cost [19,20].

Nanotechnology and nanomaterials are innovative materials for removing contaminants [21,22]. In many studies, nanoparticles have been considered to eliminate contaminants such as organic matters. Other studies also have reported that nanoparticles had remarkable efficiencies in removing pollutants [23,24].

Not only due to the very low usage and low doses of nickel oxide nanoparticles for water and wastewater treatment but also due to recycling and reuse of nanoparticles for several consecutive cycles, which has been successful according to previous studies, this nanoparticle will not have any environmental problems.

In this study, the sol-gel method was used for synthesizing NiO. It is the most commonly used technique for the preparation of bulk nanomaterial of metal oxides [21]. The method is useful to perform completely controlled reaction by the diffusion of ionic species or atomic species of reactants and products [22]. It requires high temperature and small particle size to bring the reaction partners to close sufficiently. If this method of synthesis is compared with organic chemistry where highly sophisticated synthetic routes are required, this method is crude in nature [22].

In this study, synthesized NiO nanoparticle was considered as an effective adsorbent for removing CIP from aqueous solution. The impacts of five parameters, including adsorbent dosage, pH, temperature, and adsorption time and initial concentration were scrutinized on the efficiency of CIP adsorption. Also, kinetics, isotherms and thermodynamics of CIP adsorption on synthesized NiO nanoparticles were studied.

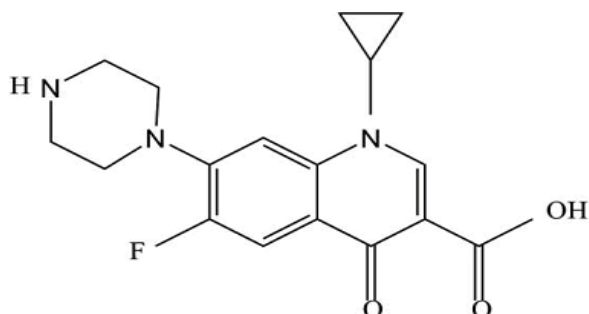


Fig. 1. Structure of ciprofloxacin.

2. Materials and methods

2.1. Materials

$\text{NH}_4\text{Cl} \cdot 6\text{H}_2\text{O}$ (CAS Number 7718-54-9), sulfuric acid (98%), sodium hydroxide (CAS Number: 1310-73-2), ethanol (96%), and hydrochloric acid (37%) were purchased from Sigma-Aldrich (USA).

Ciprofloxacin (CIP), ($\text{C}_{17}\text{H}_{18}\text{FN}_3\text{O}_3 \cdot \text{HCl}$, purity > 98%) with a molecular weight of 696.6 g/mol, was obtained from

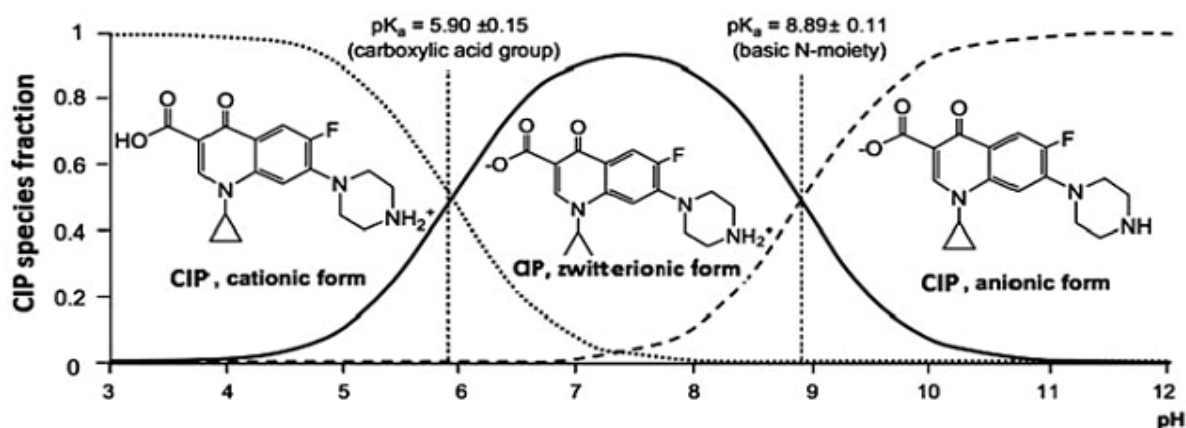


Fig. 2. Molecular structure and ionic forms of CIP as a function of pH and pK_a values.

Sigma-Aldrich (USA) and applied in the experiment without further purification. The molecular structure of CIP is given in Fig. 1. A stock solution containing 1,000 mg/L was prepared by dissolving 1 g of analytical grade CIP with distilled water in a 1 L standard flask. This was made to mark with distilled water. Standard solutions of different concentrations, as might be required, were later prepared from this stock.

2.2. Preparation of NiO nanoparticles

The nano nickel(II) oxide (NiO) was prepared using the sol-gel process [24]. Fig. 3 shows the preparation of the adsorbent by the sol-gel method. First of all, 1.5 g (0.0063 mol) $\text{NiCl}_2 \cdot 6\text{H}_2\text{O}$ was transferred to a 250 mL round bottom flask at room temperature and dissolved in 70 mL of absolute ethanol. The solution was subjected to continuous stirring. In another beaker 0.5 g (0.0125 mol) NaOH was dissolved in 100 mL absolute ethanol. This solution was added to $\text{NiCl}_2 \cdot 6\text{H}_2\text{O}$ solution dropwise. The light green colored gel was made after the mixture was stirred for 2 h. After 2 h, the gel was filtered and washed with distilled water and then finally with ethanol. The light green colored precipitate was formed. The precipitate was oven-dried at 100°C for 4 h. The fine green powder was subjected to calcination at 290°C for 30 min. Black colored nanopowder of NiO was prepared.

In the present study, to determine the shape, size, and morphology of the synthesized NiO nanoparticle, transmission electron microscopy (TEM, LEO 912 AB-100 KV, ZEISS, Germany) was used in 100 kV, and scanning electron microscopy (SEM, Mira 3 XMU, TESCAN, Czech Republic). Fourier-transform infrared (FT-IR) spectrophotometer (FTIR, Nicollet AVATAR 5700, THERMO, USA) was also used in the range of 400–4,000 cm^{-1} by applying the KBr pellet method. The surface area analyzer (Quantachrome

Corporation, USA) was used to analyze the Brunauer–Emmett–Teller (BET) surface area and porous properties, and N_2 as the adsorbate at 77 K.

2.3. Batch adsorption test

The adsorption experiment was carried out as a batch inside 250 mL Erlenmeyer flasks containing 100 mL of synthetic CIP solution. The initial pH of the samples was set by 0.1 mol NaOH and HCl in the fixed value of 3. Afterward, 1 g/L of adsorbent were added up to the solutions with CIP initial concentration of 25 mg/L. The final solution was stirred at 30°C and 120 rpm for 90 min. The solutes were filtered through filter paper and 5 mL of the solution was analyzed to measure adsorbed CIP concentration. The optimization process is repeated for other parameters. These parameters were adsorbent dosage (0.1–1.5 g/L), temperature (20°C–50°C), contact time (10–150 min), pH of aqueous solution (3–11), and initial concentration of CIP (10–100 mg/L). The temperature of the solution was adjusted to optimum condition and one of the parameters was considered as a variable while others were constant. The optimized condition of each parameter was selected and the investigation continued to define the optimum condition of other parameters. The CIP concentration was identified by high-performance liquid chromatography (C18 ODS column) with a UV detector 2006 at a wavelength of 277 nm. The mobile phase was 0.05 M phosphoric acid/acetonitrile with a volumetric ratio of 87/13 with an injection flow rate of 1 mL/min.

The amount of adsorbed ions by synthesized NiO for each gram of adsorbent is identified by Eq. (1) [25]:

$$q_e = \frac{(C_0 - C_e) \times V}{M} \quad (1)$$

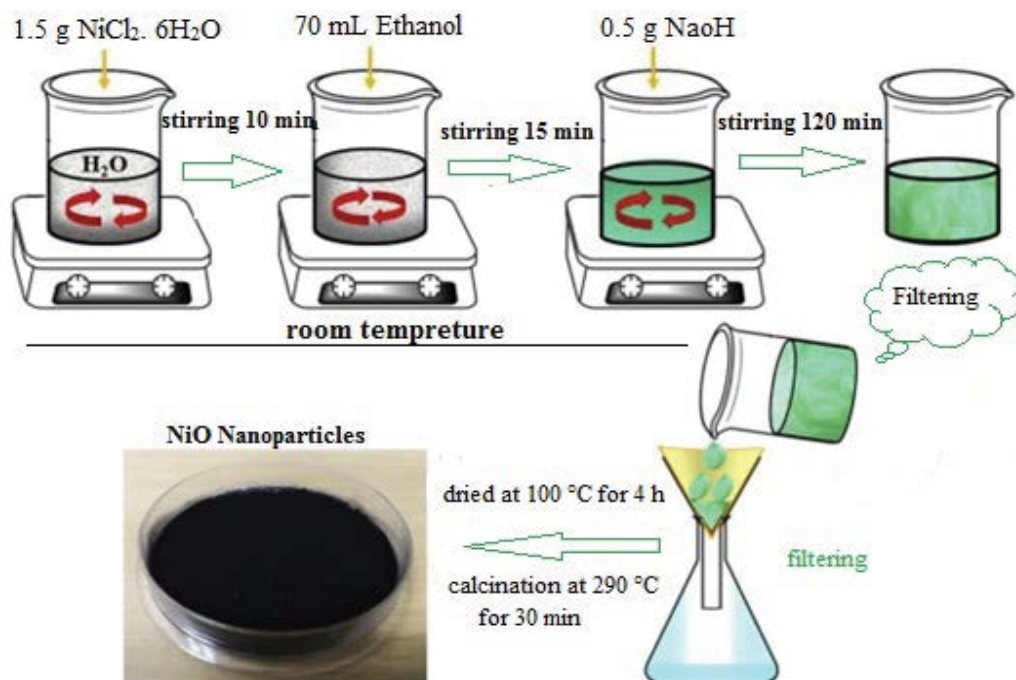


Fig. 3. Preparation of nickel oxide nanoparticles by the sol-gel method.

where q_e is the amount of CIP adsorbed per gram of adsorbent (mg/g) in the equilibrium state, C_0 and C_e are initial and equilibrium concentrations of CIP (mg/L), V is the solution volume and M is the weight of the adsorbent. In the present study, the removal of CIP in different conditions of the reaction is identified using Eq. (2) [26]:

$$\% R = \frac{(C_0 - C_e) \times 100}{C_0} \quad (2)$$

3. Results and discussion

3.1. Characteristics of synthesized NiO nanoparticle

At high magnification (50,000 \times), the nano NiO in the SEM image showed a spherical nanoparticle structure (Fig. 4a). Also, the typical TEM image of nano NiO is shown in Fig. 4b. There is a good agreement between the TEM and X-ray diffraction (XRD) results for the particle size. The average size of nano NiO, as measured by TEM, was found lower than 10 nm.

The XRD pattern of the prepared nanoparticles (Fig. 5) clearly showed the characteristic peaks of cubic NiO, which were consistent with the standard peaks of NiO (JCPDS card number 04-0835). No characteristic peaks of impurities were detected, indicating the high purity of the prepared adsorbent.

The XRD pattern of NiO nanoparticles shows five primary peaks at $2\theta = 37^\circ, 43^\circ, 63^\circ, 75^\circ,$ and 79° . As seen in Fig. 5, the diffraction peaks are broader and have weak intensity due to the small size of particles. The crystallite size of NiO nanoparticles was estimated by Debye–Scherrer equation by using Eq. (3) [27]:

$$D = \frac{K\lambda}{\beta \cos 2\theta} \quad (3)$$

The average crystallite size of synthesized NiO nanoparticles was about 9 nm.

The BET plot of nitrogen adsorption onto synthesized NiO nanoparticles are shown in Fig. 6. The specific surface area and total pore volume of synthesized NiO nanoparticles were 121.2 mg/g and 0.187 cm³/g, respectively.

The adsorption capacity obtained from this study by the cell–gel method (121.2 mg/g) is higher than the adsorption capacity obtained by the precipitation method (71.09 mg/g) and therefore one of the advantages of this method is its high adsorption capacity compared to similar methods [28].

FT-IR spectroscopy is a useful tool to understand the functional group of any organic molecule. FT-IR spectra of synthesized NiO nanoparticles are shown in Fig. 7. Metal oxides generally give absorption bands below 1,000 cm⁻¹ arising from inter-atomic vibrations. The peak at 443 cm⁻¹ in the spectrum, showing Ni–O bond, gave clear evidence about the presence of the crystalline NiO [27]. The peaks at 3,465; 1,845; and 1,386 cm⁻¹ exist, which are attributed to the adsorbed water on the products of the NiO nanoparticles. The wideband at 3,465 cm⁻¹ is mainly the stretching vibration mode O–H group and the peak at 1,621 cm⁻¹ is the O–H bending band on the surface of the products, which are associated with the adsorbed water on the products [26].

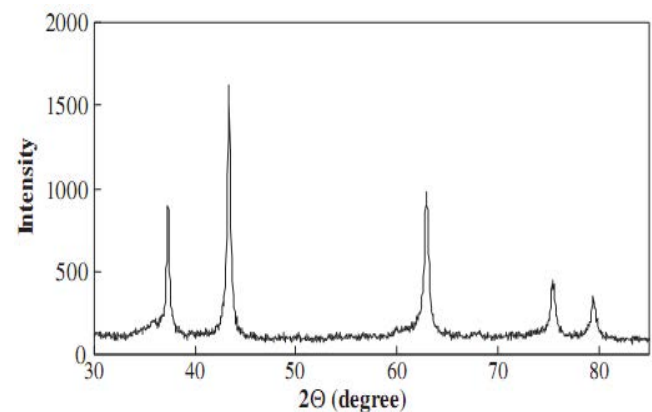


Fig. 5. XRD patterns of the synthesized NiO nanoparticle.

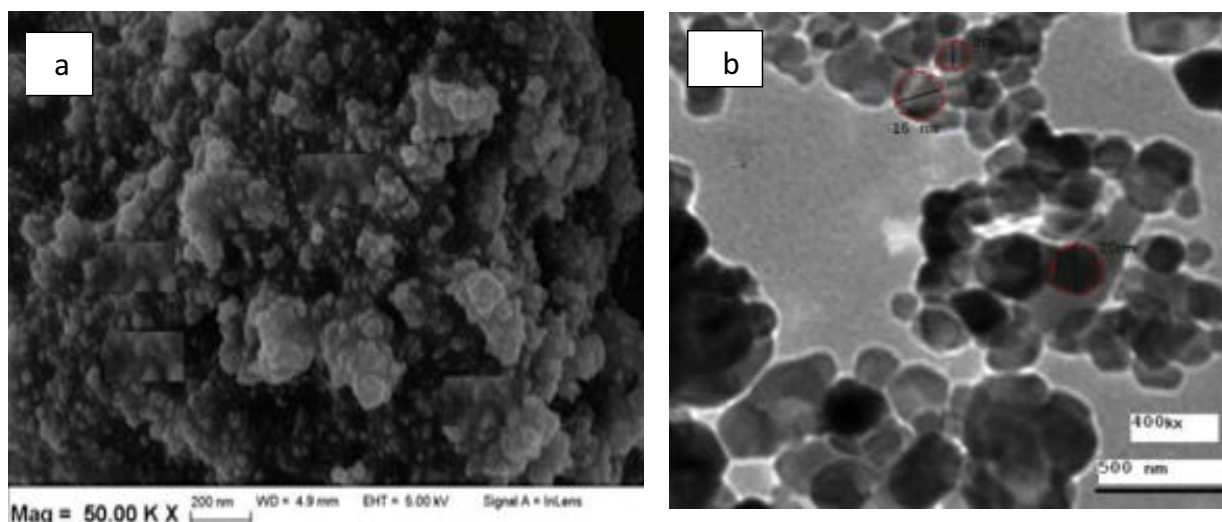


Fig. 4. (a) SEM and (b) TEM micrograph of nano NiO prepared by the sol–gel method.

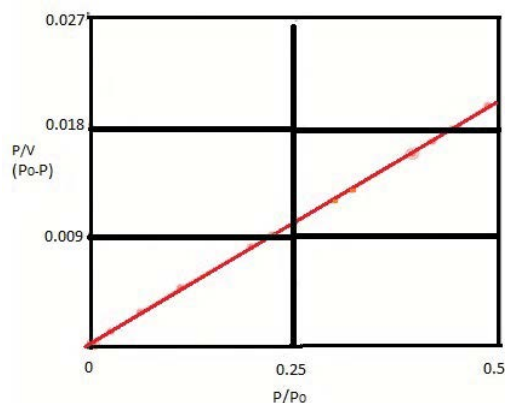


Fig. 6. BET plot of synthesized NiO nanoparticle prepared by the sol-gel method.

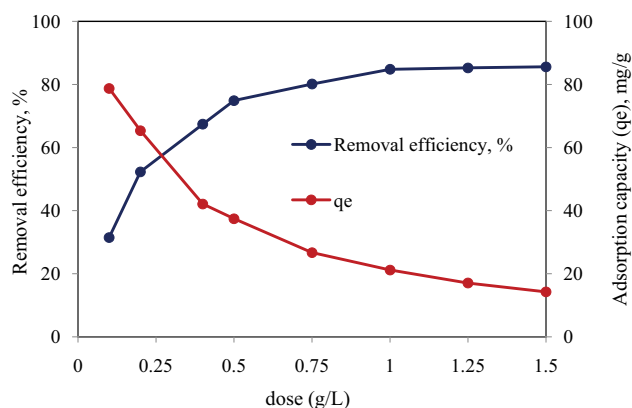


Fig. 8. Effect of adsorbent dosage on efficiency of CIP adsorption (C_0 : 25 mg/L; temperature: 30°C; pH: 7.0; time: 90 min).

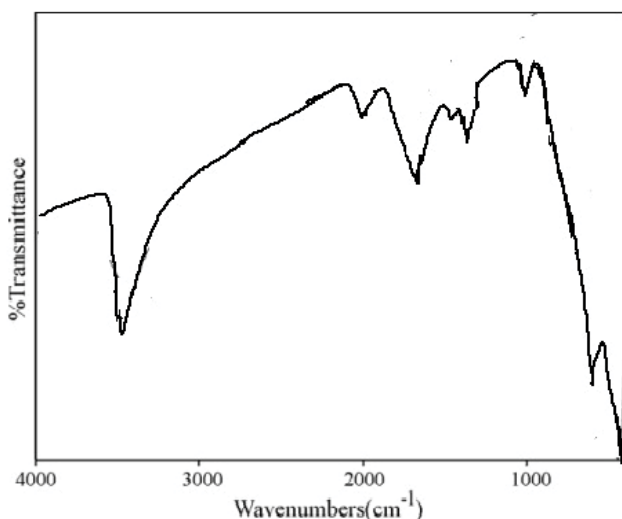


Fig. 7. FT-IR spectra of synthesized NiO nanoparticle.

3.2. Effect of synthesized NiO mass

Fig. 8 presents the result of the influence of adsorbent mass on the adsorption capacity and percentage removal of CIP. This figure reveals that adsorption efficiency was increased with the increase in the mass of the synthesized NiO nanoparticle dose up to a maximum (almost 99.2% adsorption) when the mass of the NiO dose was 1 g/L. The increase in the percentage of CIP removal with adsorbent dose could be attributed to an increase in the number of adsorption sites associated with an increase in the mass of the adsorbent and thus directly increase the surface area, as already reported in the literature [27,28]. Conversely, the adsorption capacity of the synthesized NiO decreased gradually from 93.1 to 16.5 mg/g when the mass of synthesized NiO dose was increased from 0.1 to 1.5 g. This observation can be linked to the concentration gradient [29,30].

By increasing the dosage of adsorbent, the adsorption sites of adsorbent could not be full-scaled used and made some adsorption sites approached, so that the adsorption capacity of per unit of adsorbent gradually reduced.

In general, the surface area and available sites are usually related to the amount of adsorbent [24].

3.3. Effect of pH on the removal of CIP

In order to study the effect of pH on CIP adsorption, 25 mg/L CIP solution was shaken with 1 g/L synthesized NiO and equilibrated for 90 min at pH values ranging from 3.0 to 11.0. Comparing the removal efficiency at different pH, the adsorbed CIP decreased with increasing pH (Fig. 9). CIP pKa values were 6.1 and 8.7 for the carboxylic acid group and amine group on the piperazine moiety, respectively [11]. When the pH of the solution is below 6.1, CIP is mainly present as a cation, but CIP exists in zwitterionic form when pH ranges from 6.1 to 8.7. If the pH of the solution is above 8.7, CIP loses protons from the carboxylic group and is mainly in anion form [9,10]. When the pH was lower than 6, removal of CIP increased because of improved electrostatic attraction which results from the opposite charge between the CIP and synthesized NiO nanoparticles. In contrast, at high pH, CIP removal was significantly reduced. This may be due to the zwitterionic nature of CIP. In acidic solutions, ionic interactions between CIP and the adsorbent surface occur, which causes high removal efficiencies [12,13].

3.4. Effect of contact time and initial concentration of CIP

The result of contact time on the removal of CIP by synthesized NiO is presented in Fig. 10. The result shows that the rate of CIP removal occurred rapidly within the first 30 min of the adsorption and therefore proceeded to an equilibrium state with the maximum percentage removal of 99.2%. This indicates that most of the adsorption occurs on the surface rather than the pores of the synthesized NiO nanoparticle [30,31]. This further confirms that the adsorption of CIP by synthesized NiO was physical in nature [32].

Also as shown in Fig. 10 the adsorption rate was rapidly increasing at the beginning of the adsorption process and gradually decreased with the lengthen of contact time until adsorption equilibrium. This was because the mass concentration of the CIP in the solution was high at the

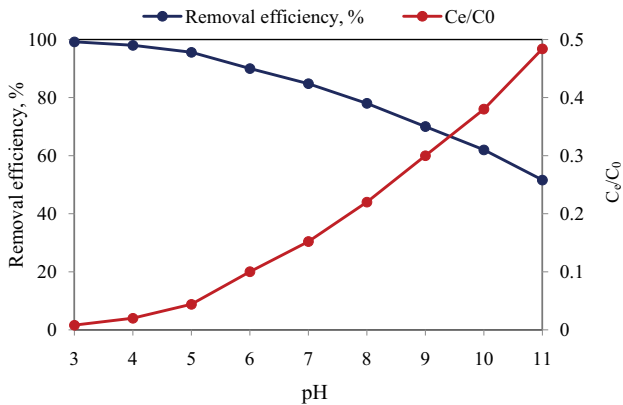


Fig. 9. Effect of initial pH on efficiency of CIP adsorption (C_0 : 25 mg/L; temperature: 30°C; time: 90 min; adsorbent dosage: 1 g/L).

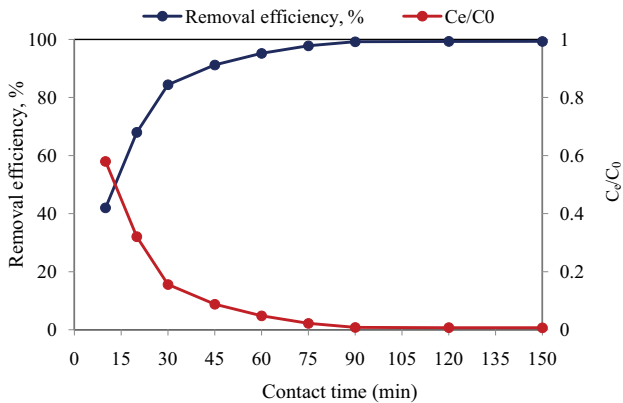


Fig. 10. Effect of contact time on the efficiency of CIP adsorption (C_0 : 25 mg/L; temperature: 30°C; pH: 3; adsorbent dosage 1 g/L).

beginning time, and there were a large amount of available adsorption sites of synthesized NiO. As the adsorption proceeding, the decreasing adsorption rate gradually decreased due to the adsorption sites were gradually occupied by CIP ions [31].

The effect of the initial concentration of the CIP on adsorption amounts depends on the synthesized NiO nanoparticles which were investigated by changing the concentrations in aqueous solution in the range of 10–100 mg/L. Fig. 11 shows the effect of the initial concentrations of CIP on adsorption capacities. As observed in the graphs, the amount of CIP adsorbed by the synthesized NiO nanoparticles that were increased with the increasing CIP concentration. This may be because the amount of CIP ions obtainable for adsorption increases with the increase in initial concentrations [33].

3.5. Kinetic studies

Pseudo-first-order, pseudo-second-order, and intraparticle diffusion models have been used for kinetic data in different systems. The pseudo-first-order equation is expressed as following [33,34]:

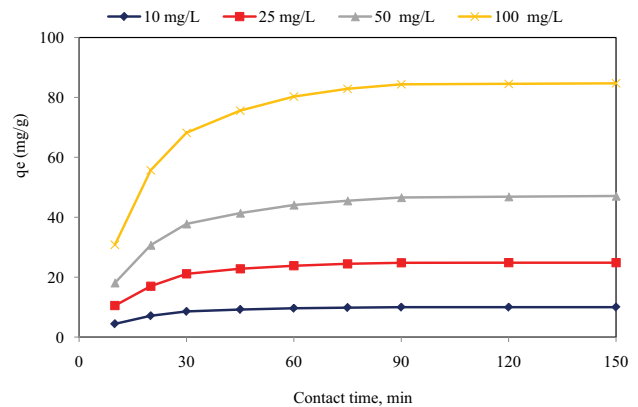


Fig. 11. Effect of initial concentration on the efficiency of CIP adsorption (temperature: 30°C; pH: 3; adsorbent dosage 1 g/L).

$$\log(q_e - q_t) = \log q_e - \frac{K_1}{2.303} t \quad (4)$$

where q_t (mg CIP/g adsorbent) is the amount of adsorbed solute, q_e (mg CIP/g adsorbent) is CIP concentrations at equilibrium, K_1 (min^{-1}) is the pseudo-first-order rate constant and t (min) is time. The q_e and K_1 can be obtained by linear regression. That is, a linear regression line is formed by plotting $\log(q_e - q_t)$ vs. t , where K_1 and q_e are the slope and intercept of the line, respectively.

K_1 is used to determine the rate of equilibrium in the system and is both ways dependent and independent of the conditioned systems. That is, K_1 is a combination of adsorption and desorption rate constants and is not the intrinsic adsorption rate constant.

The most commonly used pseudo-second-order equation in the form of Eq. (5) [35,36]:

$$\frac{t}{q_t} = \frac{1}{h} + \frac{t}{q_e} \quad (5)$$

where $h = K_2 q_e^2$ can be regarded as the initial adsorption rate when $t \rightarrow 0$ and K_2 (g adsorbent/mg CIP min) is a constant which is strongly dependent on the applied operating conditions. For instance, K_2 is highly dependent on initial solute concentrations. The pseudo-second-order model includes the presumption that the rate-limiting step refers to chemical adsorption which occurs by sharing or exchange of electrons between adsorbent and adsorbate. It is presumed that the adsorption capacity increases in the proportion to the number of active sites of the adsorbed materials.

The intraparticle diffusion model is expressed as (Eq. (6)) [37]:

$$q_t = K_d t^{0.5} + I \quad (6)$$

where K_d ($\text{mg/g min}^{0.5}$) is the rate constant for intraparticle diffusion and I represent the thickness of the boundary layer. The values of K_d and I correspond to the slope and intercept of the plot of q_t vs. $t^{0.5}$, which indicates a multilinearity,

suggesting that the adsorption processes include multiple steps. Solute adsorption by porous adsorbents consists of three consecutive steps. The first step means external or improvisational adsorption. The second step refers to the gradual adsorption that occurs when intraparticle diffusion is rate-limiting. The last step is the final equilibrium stage when intraparticle diffusion slows down due to a markedly lower adsorbate concentration. The intraparticle diffusion is the rate-limiting step when the regression line passes through the origin. In contrast, when the regression line does not go by origin, besides intraparticle diffusion, other processes can control the adsorption efficiency [38].

The K_d values increased with increasing initial concentration (Table 1), suggesting a greater driving force as the initial concentration increased.

Table 1 indicates that the calculated q_e of the pseudo-second-order model was more similar to the value obtained from the actual experiment than the calculated q_e of the pseudo-first-order model. In addition, R^2 values of the pseudo-second-order model (Fig. 12) were higher than those of the pseudo-first-order model. Thus, the pseudo-second-order model fits better than the pseudo-first-order model. The reaction may not be a pseudo-first-order reaction despite a high correlation coefficient if the experimental q_e is not equal to the intercept. For this adsorbent, experimental data was not fit to pseudo-first-order kinetic due to $q_{e,cal}$ values calculated by pseudo-first-order kinetic are not equal to $q_{e,exp}$. Generally, the rate constant (K_2) decreases for larger concentrations due to the limited adsorption sites

on synthesized NiO nanoparticle, and when the initial concentration is an increase from 10 to 100 mg/L, K_2 value is decreased from 0.0089 to 0.0012 (g/mg min).

As shown in Fig. 13, the plots showed multi-linear, suggesting that there were two or more steps while the adsorption process occurred. The first stage occurred from 0 to 30 min and represented the transport of CIP molecules from the external surface of the adsorbents to the internal pores of the adsorbents. The second linear portion included the adsorption period from 30–60 min, which represents intraparticle diffusion. The third stage took place between 60 and 90 min and adsorption of CIP molecules occurred on the interior surface of the adsorbent. The third stage reflected a very low slope due to the decrease in CIP concentrations and available active sites [39]. This means the equilibrium adsorption is almost reached.

3.6. Adsorption thermodynamics

Adsorption of CIP onto synthesized NiO nanoparticles can be influenced by temperature; thus, adsorption experiments were conducted at various temperatures (20°C, 30°C, 40°C, and 50°C). The removal efficiency increased from 86.4% to 99.2% with increasing temperature. This is because of an increase in the number of sorption sites which results from a breakdown of some internal bond of the active surface of the adsorbent [31]. Thermodynamic parameters were estimated to study the thermodynamic properties of CIP adsorption. Also, the relationship

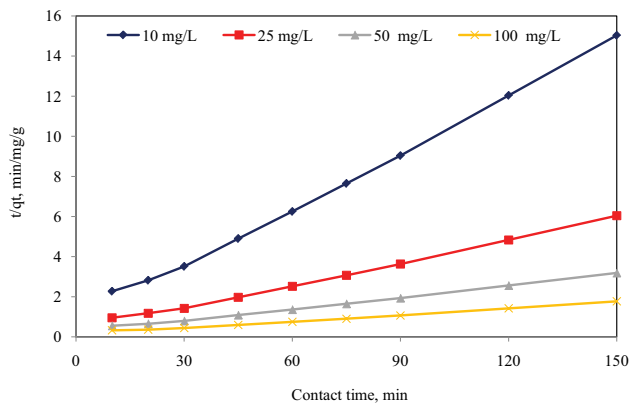


Fig. 12. Pseudo-second-order plots for the kinetic modeling of CIP adsorbed onto NiO nanoparticle at different concentrations.

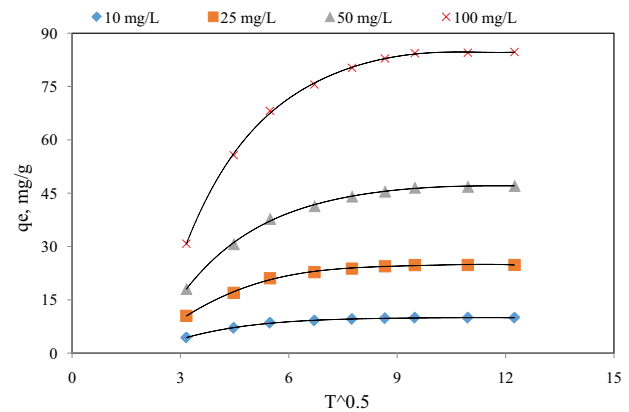


Fig. 13. Intraparticle diffusion plots for the kinetic modeling of CIP adsorbed onto NiO nanoparticle at different concentrations.

Table 1 Results of kinetic model related to the CIP adsorption onto NiO nanoparticle

CIP concentration (mg/L)	$q_{e,exp}$	Intraparticle diffusion model			Pseudo-first-order			Pseudo-second-order		
		K_d	I	R^2	$q_{e,cal}$	K_1	R^2	$q_{e,cal}$	K_2	R^2
10	9.981	0.819	11.82	0.792	3.127	0.029	0.895	9.064	0.0089	0.998
25	24.82	0.711	14.71	0.814	8.341	0.038	0.912	22.73	0.0068	0.997
50	47.09	0.521	19.52	0.786	14.36	0.059	0.904	41.35	0.0047	0.999
100	84.72	0.307	21.46	0.788	29.34	0.076	0.876	81.64	0.0012	0.997

between the CIP distribution coefficient (K_e) and free energy (ΔG° kJ/mol) of adsorption (Eq. (7)) is [40,41]:

$$\Delta G^\circ = -RT \ln K_e \quad (7)$$

The equilibrium constant K_e was calculated from the concentration of CIP adsorbed at equilibrium ($C_0 - C_e$) and equilibrium concentration (C_e) of the CIP in the liquid phase using the following equation [34]:

$$K_e = \frac{(C_0 - C_e)}{C_e} \quad (8)$$

The van't Hoff Eqs. (9) and (10) was employed to compute the values ΔH° and ΔS° from the equilibrium constant as shown [37,38]:

$$\log\left(\frac{1}{C_e}\right) = \log K_e + \left(\frac{-\Delta H^\circ}{2.303RT}\right) \quad (9)$$

$$\Delta S^\circ = \frac{\Delta H^\circ - \Delta G^\circ}{T} \quad (10)$$

where ΔH° is the enthalpy change, ΔS° is the entropy change, t is the temperature in Kelvin and R is the gas constant (kJ/mol K). Table 2 indicates the thermodynamic parameters obtained from experimental data. The negative value of ΔG° means that Gibb's free energy decreases, suggesting that the adsorption processes are feasible and spontaneous [32]. The positive value of ΔH° suggests the endothermic nature of adsorption [35]. Based on the positive value of ΔS° , we concluded that some structural changes occur on the adsorbent and the randomness increased at solid/liquid interface [37].

3.7. Adsorption isotherms

Adsorption isotherms can depict the interaction between adsorbate and adsorbent. Langmuir adsorption isotherm is known to model a single coating layer on surface adsorption. Furthermore, the surface of the adsorbent is homogeneous; as a result, adsorption energy is the same on all active sites. Langmuir isotherm is expressed following [42]:

$$\frac{C_e}{q_e} = \frac{1}{q_m K} + \frac{C_e}{q_m} \quad (11)$$

Table 2
Values of thermodynamic parameters for the adsorption of CIP onto synthesized NiO nanoparticle

Temperature (K)	ΔG° (kJ/mol)	ΔH° (kJ/mol)	ΔS° (J/mol K)
293	-4.354	6.928	38.5
303	-5.065	7.491	41.4
313	-5.971	7.916	44.3
323	-6.284	8.241	44.9

where q_m is the monolayer capacity, K is the equilibrium constant. These constants can be determined from the intercept and the slope of the linear plot of experimental data of C_e/q_e vs. C_e . Another effective parameter in the Langmuir equation is R_L that describes the properties of the equation. The value of R_L is the representative of the state and quality of the adsorption isotherm model. If $R_L > 1$, $R_L = 0$, $R_L = 1$ and $0 < R_L < 1$, the process is non-desired, irreversible, linear and desirable, respectively. The value of R_L is identified using Eq. (12) [43].

$$R_L = \frac{1}{1 + KC_0} \quad (12)$$

Freundlich isotherm is used for modeling the adsorption which occurs on heterogeneous surfaces. The linear expression of Freundlich isotherm is given by Eq. (13) [44]:

$$\log q_e = \log K_F + \frac{1}{n} \log C_e \quad (13)$$

where K_F is the constant indicating adsorption capacity of the adsorbent, and n represents the constant related to the adsorption intensity. K_F and n were estimated from the slope and intercept of the plot of $\log q_e$ vs. $\log C_e$. The plot of $\log q_e$ vs. $\log C_e$ can give linear regression with slope and intercept, corresponding to K_F and n , respectively. Values of $n > 1$ indicate favorable adsorption as a physical process. When n is equal to 1, adsorption is linear, but adsorption is a chemical process when n is below 1.

Temkin isotherm has one factor which shows the interaction between adsorbent and adsorbing particle so vividly. This model was applied in forms, given as Eq. (14) [45]:

$$q_e = B \ln K_T + B \ln C_e \quad (14)$$

where B is Temkin constant which is related to the heat of sorption (J/mol) and K_T is Temkin isotherm constant (L/g). Plotting of q_e vs. $\ln(C_e)$ gives a linear line of slope RT/b and intercept $(RT \ln K_T)/b$.

Dubinin–Radushkevich (D-R) isotherm model is an empirical model that is applied to represent the adsorption processed with Gaussian energy distribution onto heterogeneous surfaces. This isotherm applies only when adsorbate concentrations are moderate, and is expressed as follows [46]:

$$\log q_e = \ln q_m - \beta \varepsilon^2 \quad (15)$$

where q_e is the amount of adsorbate in the adsorbent at equilibrium (mg/g), q_m is theoretical isotherm saturation capacity (mg/g), β is D-R isotherm constant (mol²/kJ²). $\varepsilon =$ D-R isotherm constant. This approach was used to distinguish the physical and chemical adsorption of metals with its free energy (E), which can be computed by the relationship [47]:

$$E = \left[\frac{1}{2\beta} \right] \quad (16)$$

$$\varepsilon = RT \ln \left[1 + \frac{1}{C_e} \right] \tag{17}$$

where R = the gas constant (8.314 J/mol K); T = absolute temperature (K); C_e = adsorbate equilibrium concentration (mg/L).

The Redlich–Peterson (R-P) isotherm model is applied to indicate adsorption equilibrium for a wide concentration range, and is suitable for either homogeneous or heterogeneous systems.

It can be described by Eq. (18) [48]:

$$\ln \left[K_R \frac{C_e}{q_e} - 1 \right] = \ln a_R + \beta \ln C_e \tag{18}$$

where K_R is the R-P constant (L/g), a_R is the R-P constant (L/mg) and β is the exponent which lies between 1 and 0.

The Langmuir, Freundlich, R-P, Temkin, D-R and R-P isotherm parameters were determined through the linearized form and their values, along with the respective correlation coefficients, and are listed in Table 3. This table shows that the best correlation coefficients were, in decreasing order, Langmuir > R-P > Temkin > D-R > Freundlich models. Table 3 also shows that q_m values of the Langmuir and D-R isotherm models increased with increasing at temperature. Also, Table 3 shows that energy values of CIP sorption increased from 2.75 to 9.65 kJ/mol with a temperature increase from 293 to 323 K and indicate that physisorption played a significant role in the adsorption process at low temperatures [45]. Values of R_L were observed to be between 0 and 1 in this study (Table 3); thus, the adsorption was fairly favorable and the adsorbent used in this study had good potential for CIP removal.

Table 4 shows a comparison of the adsorption capacity (q_e) of different materials reported in the literatures as adsorbent for CIP adsorption from aqueous solution under different experimental conditions. The results demonstrated that the synthesized NiO can be a promising material for removal of CIP from pharmaceutical wastewater.

4. Conclusion

In this study, we have studied the removal of CIP from aqueous solution using synthesized NiO over a wide

range of concentrations. The influence of several factors (e.g., temperature, adsorbent dosage, contact time, pH, and initial CIP concentrations) on the removal of CIP by synthesized NiO were tested. The following conclusions are made based on the results of the present study:

- Thermodynamic parameters indicated that CIP adsorption was endothermic adsorption. The negative values of ΔG° indicated the spontaneous nature of the adsorption.
- Adsorption of CIP increased with contact time and adsorbent dose at a certain limit.
- Optimum pH was shown to be 3.0 with the removal rate reaching 99.2%.

Table 3
Isotherm parameters for adsorption of CIP onto synthesized NiO nanoparticle at various temperatures

Isotherm models	293°K	303°K	313°K	323°K
Langmuir				
q_m (mg/g)	84.72	87.9	91.35	94.26
K (L/mg)	0.0245	0.289	0.0321	0.237
R_L	0.0384	0.206	0.0412	0.195
R^2	0.996	0.998	0.998	0.997
Freundlich				
K_F	17.44	19.25	20.61	21.14
n	2.761	2.925	3.136	3.425
R^2	0.745	0.761	0.756	0.784
Temkin				
K_T	0.724	0.819	0.966	1.145
B	11.76	14.95	17.14	18.41
R^2	0.885	0.871	0.872	0.896
Dubinin–Radushkevich				
q_m (mg/g)	46.86	57.25	69.34	74.81
E	2.751	5.592	7.249	9.654
R^2	0.827	0.846	0.852	0.868
R-P				
K_R (L/g)	6.241	7.584	8.972	10.46
a_R (L/mg)	0.848	1.142	1.346	1.679
R^2	0.925	0.936	0.944	0.962

Table 4
Comparison of the maximum adsorption of various adsorbent for CIP

Adsorbents	q_e (mg/g)	References	Adsorbents	q_e (mg/g)	References
AC-palm leaflets	48.91	[9]	AC-Jerivá	65.9	[10]
Graphene	71.11	[12]	Granular AC	38.49	[12]
Schorl	56.95	[13]	Goethite	74.28	[11]
MgO nanoparticles	84.93	[14]	CuO nanoparticles	89.46	[15]
Microwave pyrolysis	93.16	[18]	MWCNT	102.75	[23]
Birnessite	66.79	[25]	Bamboo charcoal	59.35	[26]
Synthesized NiO	Temperature 293°K = 84.72 Temperature 303°K = 87.9	This study	Synthesized NiO	Temperature 313°K = 91.35 Temperature 323°K = 94.26	This study

- Based on R^2 values and comparison of calculated and experimental q_e values, the kinetic data represented that CIP adsorption follows the second-order kinetic models.
- Isotherm data indicated that the adsorption of CIP onto the synthesized NiO followed the Langmuir isotherm model with a maximum adsorption capacity of 94.26 mg/g at 50°C.
- Results demonstrated that the synthesized NiO can be a promising material for the removal of CIP from pharmaceutical wastewater.

Acknowledgments

The authors are grateful to the Zahedan University of Medical Sciences for the financial support of this study (Project No. 9162). This research was also supported by the Basic Science Research Program through the National Research Foundation of Korea (NRF) funded by the Ministry of Education (NRF-2019R111A3A01062424).

References

- [1] M.Y. Badi, A. Azari, H. Pasalari, A. Esrafil, M. Farzadkia, Modification of activated carbon with magnetic Fe_3O_4 nanoparticle composite for removal of ceftriaxone from aquatic solutions, *J. Mol. Liq.*, 261 (2016) 146–154.
- [2] H. Azarpira, Y. Mahdavi, O. Khaleghi, D. Balarak, Thermodynamic studies on the removal of metronidazole antibiotic by multi-walled carbon nanotubes, *Pharm Lett.*, 8 (2016) 107–113.
- [3] S. Abbasi, R. Foroutan, H. Esmaeili, F. Esmaeilzadeh, Preparation of activated carbon from worn tires for removal of Cu(II), Ni(II) and Co(II) ions from synthetic wastewater, *Desal. Water Treat.*, 141 (2019) 269–278.
- [4] M. Keshavarz, R. Foroutan, F. Papari, L. Bulgariu, H. Esmaeili, Synthesis of $\text{CaO}/\text{Fe}_2\text{O}_3$ nanocomposite as an efficient nanoadsorbent for the treatment of wastewater containing Cr(III), *Sep. Sci. Technol.*, 11 (2020) 1–14.
- [5] S. Nasser, A.H. Mahvi, M. Seyedsalehi, K. Yaghmaei, R. Nabizadeh, M. Alimohammadi, G.H. Safari, Degradation kinetics of tetracycline in aqueous solutions using peroxydisulfate activated by ultrasound irradiation: effect of radical scavenger and water matrix, *J. Mol. Liq.*, 241 (2017) 704–714.
- [6] R. Rostamian, H. Behnejad, A comparative adsorption study of sulfamethoxazole onto graphene and graphene oxide nanosheets through equilibrium, kinetic and thermodynamic modeling, *Process Saf. Environ. Prot.*, 102 (2016) 20–29.
- [7] Z. Movasaghi, B. Yan, C. Niu, Adsorption of ciprofloxacin from water by pretreated oat hulls: equilibrium, kinetic, and thermodynamic studies, *Ind. Crops Prod.*, 127 (2016) 237–250.
- [8] Ö. Kerkez-Kuyumcu, Ş.S. Bayazit, M.A. Salam, Antibiotic amoxicillin removal from aqueous solution using magnetically modified graphene nanoplatelets, *J. Ind. Eng. Chem.*, 35 (2016) 198–205.
- [9] E.-S.I. El-Shafey, H. Al-Lawati, A.S. Al-Sumri, Ciprofloxacin adsorption from aqueous solution onto chemically prepared carbon from date palm leaflets, *J. Environ. Sci.*, 24 (2012) 1579–1586.
- [10] C. de O. Carvalho, D.L.C. Rodrigues, É.C. Lima, C.S. Umpierrez, D.F.C. Chaguezac, F.M. Machado, Kinetic, equilibrium, and thermodynamic studies on the adsorption of ciprofloxacin by activated carbon produced from Jerivá (*Syagrus romanzoffiana*), *Environ. Sci. Pollut. Res. Int.*, 26 (2019) 4690–4702.
- [11] S.T. Danalioğlu, S.S. Bayazit, O.K. Kuyumcu, M.A. Salam, Efficient removal of antibiotics by a novel magnetic adsorbent: magnetic activated carbon/chitosan (MACC) nanocomposite, *J. Mol. Liq.*, 240 (2017) 589–596.
- [12] X. Zhu, D.C.W. Tsang, F. Chen, S.Y. Li, X. Yang, Ciprofloxacin adsorption on graphene and granular activated carbon: kinetics, isotherms, and effects of solution chemistry, *Environ. Technol.*, 36 (2015) 3094–3102.
- [13] D.Y. Yin, Z.W. Xu, J. Shi, L. Shen, Z.X. He, Adsorption characteristics of ciprofloxacin on the schorl: kinetics, thermodynamics, effect of metal ion and mechanisms, *J. Water Reuse Desal.*, 8 (2017) 350–359.
- [14] A. Fakhri, S. Adami, Adsorption and thermodynamic study of Cephalosporins antibiotics from aqueous solution onto MgO nanoparticles, *J. Taiwan Inst. Chem. Eng.*, 45 (2014) 1001–1006.
- [15] N. Sharma, N. Dhiman, Kinetic and thermodynamic studies for ciprofloxacin hydrochloride adsorption from aqueous solution on CuO nanoparticles, *Int. J. ChemTech Res.*, 10 (2017) 98–106.
- [16] R. Ding, P.F. Zhang, M. Sereych, T.J. Badosz, Removal of antibiotics from water using sewage sludge- and waste oil sludge-derived adsorbents, *Water Res.*, 90 (2012) 40–6.
- [17] D. Balarak, H. Azarpira, F.K. Mostafapour, Study of the adsorption mechanisms of cephalixin on to *Azolla filiculoides*, *Pharm. Chem.*, 8 (2016) 114–121.
- [18] M.J. Ahmed, S.K. Theydan, Fluoroquinolones antibiotics adsorption onto microporous activated carbon from lignocellulosic biomass by microwave pyrolysis, *J. Taiwan Inst. Chem. Eng.*, 45 (2014) 219–226.
- [19] K.-J. Choi, S.-G. Kim, S.-H. Kim, Removal of antibiotics by coagulation and granular activated carbon filtration, *J. Hazard. Mater.*, 151 (2008) 38–43.
- [20] T.X. Bui, H. Choi, Adsorptive removal of selected pharmaceuticals by mesoporous silica SBA-15, *J. Hazard. Mater.*, 168 (2009) 602–608.
- [21] D. Balarak, F.K. Mostafapour, E. Bazrafshan, T.A. Saleh, Studies on the adsorption of amoxicillin on multi-wall carbon nanotubes, *Water Sci. Technol.*, 75 (2017) 1599–1606.
- [22] L.G. Ji, W. Chen, L. Duan, D.Q. Zhu, Mechanisms for strong adsorption of tetracycline to carbon nanotubes: a comparative study using activated carbon and graphite as adsorbents, *Environ. Sci. Technol.*, 43 (2009) 2322–2327.
- [23] S.A.C. Carabineiro, T. Thavorn-amornsri, M.F.R. Pereira, P. Serp, J.L. Figueiredo, Comparison between activated carbon, carbon xerogel and carbon nanotubes for the adsorption of the antibiotic ciprofloxacin, *Catal. Today*, 186 (2012) 29–34.
- [24] V. Srivastava, Y.C. Sharma, M. Sillanpää, Application of response surface methodology for optimization of Co(II) removal from synthetic wastewater by adsorption on NiO nanoparticles, *J. Mol. Liq.*, 211 (2015) 613–620.
- [25] W.-T. Jiang, P.-H. Chang, Y.-S. Wang, Y. Tsai, J.-S. Jean, Z.H. Li, K. Krukowski, Removal of ciprofloxacin from water by birnessite, *J. Hazard. Mater.*, 250 (2013) 362–369.
- [26] L. Wang, G.C. Chen, C. Ling, J.F. Zhang, K. Szerlag, Adsorption of ciprofloxacin on to bamboo charcoal: effects of pH, salinity, cations, and phosphate, *Environ. Prog. Sustainable Energy*, 36 (2017) 1108–1115.
- [27] U. Ashraf, B. Khan, Synthesis and characterization of NiO nanopowder by sol-gel method, *Int. J. Sci. Res.*, 4 (2015) 2405–2408.
- [28] S.K. Ashan, N. Ziaefara, M. Khosravi, Sol-gel synthesis of NiO nanoparticles and investigation on adsorption capacity in the removal of Cr(VI) from aqueous solution, *Orient. J. Chem.*, 32 (2016) 749–758.
- [29] A.K. Rahardjo, M.J.J. Susanto, A. Kurniawan, N. Indraswati, S. Ismadji, Modified Ponorogo bentonite for the removal of ampicillin from wastewater, *J. Hazard. Mater.*, 190 (2011) 1001–1008.
- [30] H. Azarpira, D. Balarak, Rice husk as a biosorbent for antibiotic metronidazole removal: isotherm studies and model validation, *Int. J. ChemTech Res.*, 9 (2016) 566–573.
- [31] M. Brigante, P.C. Schulz, Removal of the antibiotic tetracycline by titania and titania-silica composed material, *J. Hazard. Mater.*, 192 (2011) 1597–1608.
- [32] R. Ocampo-Pérez, J. Rivera-Utrilla, C. Gómez-Pacheco, M. Sánchez-Polo, J.J. López-Peñalver, Kinetic study of tetracycline

- adsorption on sludge-derived adsorbents in aqueous phase, Chem. Eng. J., 213 (2012) 88–96.
- [33] I.O. Abdulsalam, H.I. Adegoke, F.A. Adekola, Batch sorption of ciprofloxacin on kaolinitic clay and nhematite composite: equilibrium and thermodynamics studies, Mor. J. Chem., 4 (2016) 384–424.
- [34] A.H. Mahvi, F.K. Mostafapour, Biosorption of tetracycline from aqueous solution by *Azolla filiculoides*: equilibrium kinetic and thermodynamics studies, Fresenius Environ. Bull., 27 (2018) 5759–5767.
- [35] L. Zhang, X.Y. Song, X.Y. Liu, L.J. Yang, F. Pan, J. Lv, Studies on the removal of tetracycline by multi-walled carbon nanotubes, Chem. Eng. J., 178 (2011) 26–33.
- [36] P.-H. Chang, Z.H. Li, J.-S. Jean, W.-T. Jiang, C.-J. Wang, K.-H. Lin, Adsorption of tetracycline on 2:1 layered non-swelling clay mineral illite, Appl. Clay Sci., 67–68 (2012) 158–163.
- [37] Y. Gao, Y. Li, L. Zhang, H. Huang, J.J. Hu, S.M. Shah, X.G. Su, Adsorption and removal of tetracycline antibiotics from aqueous solution by graphene oxide, J. Colloid Interface Sci., 368 (2012) 540–546.
- [38] L. Wang, G.C. Chen, G. Owens, J.F. Zhang, Enhanced antibiotic removal by the addition of bamboo charcoal during pig manure composting, RSC Adv., 6 (2016) 27575–27583.
- [39] M.E. Parolo, M.C. Savini, J.M. Vallés, M.T. Baschini, M.J. Avena, Tetracycline adsorption on montmorillonite: pH and ionic strength effects, Appl. Clay Sci., 40 (2008) 179–186.
- [40] I. Yahiaoui, F. Aissani-Benissad, F. Fourcade, A. Amrane, Removal of tetracycline hydrochloride from water based on direct anodic oxidation (Pb/PbO₂ electrode) coupled to activated sludge culture, Chem. Eng. J., 221 (2013) 418–425.
- [41] D. Balarak, F.K. Mostafapour, H. Azarpira, Adsorption isotherm studies of tetracycline antibiotics from aqueous solutions by maize stalks as a cheap biosorbent, Int. J. Pharm. Technol., 8 (2016) 16664–16675.
- [42] N. Khoshnamvand, S. Ahmadi, F.K. Mostafapour, Kinetic and isotherm studies on ciprofloxacin an adsorption using magnesium oxide nanoparticles, J. Appl. Pharm. Sci., 7 (2017) 79–83.
- [43] C.-L. Zhang, G.-L. Qiao, F. Zhao, Y. Wang, Thermodynamic and kinetic parameters of ciprofloxacin adsorption onto modified coal fly ash from aqueous solution, J. Mol. Liq., 163 (2011) 53–56.
- [44] S. Rakshit, D. Sarkar, E.J. Elzinga, P. Punamiya, R. Datta, Mechanisms of ciprofloxacin removal by nano-sized magnetite, J. Hazard. Mater., 246 (2013) 221–226.
- [45] W.R.D.N. Sousa, A.R. Oliveira, J.F.C. Filho, T.C.M. Dantas, A.G.D. Santos, V.P.S. Caldeira, G.E. Luz Jr., Ciprofloxacin adsorption on ZnO supported on SBA-15, Water Air Soil Pollut., 229 (2018) 1–12.
- [46] S. Tamjidi, H. Esmaeili, B.K. Moghadas, Application of magnetic adsorbents for removal of heavy metals from wastewater: a review study, Mater. Res. Express, 6 (2019) 1–9.
- [47] S. Ahmadi, A. Banach, F.K. Mostafapour, Study survey of cupric oxide nanoparticles in removal efficiency of ciprofloxacin antibiotic from aqueous solution: adsorption isotherm study, Desal. Water Treat., 89 (2017) 297–303.
- [48] D. Balarak, E. Bazrafshan, Y. Mahdavi, S.-M. Lee. Kinetic, isotherms and thermodynamic studies in the removal of 2-chlorophenol from aqueous solution using modified rice straw, Desal. Water Treat., 63 (2017) 203–211.